Applied Physics Letters ARTICLE pubs.aip.org/aip/apl

Source of two-dimensional electron gas in unintentionally doped AlGaN/GaN multichannel high-electron-mobility transistor heterostructures—Experimental evidence of the hole trap state

Cite as: Appl. Phys. Lett. **123**, 092105 (2023); doi: 10.1063/5.0147392
Submitted: 22 February 2023 · Accepted: 17 August 2023 ·
Published Online: 1 September 2023

R. Lingaparthi,[1,a] N. Dharmarasu,[1] K. Radhakrishnan,[1,2,3,b] and Lili Huo[3]

AFFILIATIONS

[1]Temasek Laboratories, Nanyang Technological University, Singapore 637553
[2]Center for Micro/Nano-electronics (CMNE), School of Electrical and Electronic Engineering, Nanyang Technological University, Singapore 639798
[3]UMI3288 CINTRA, (CNRS/NTU/THALES), Nanyang Technological University, Research Techno Plaza, 50 Nanyang Drive, Singapore 637553

[a]Electronic mail: ravikira1@e.ntu.edu.sg
[b]Author to whom correspondence should be addressed: eradha@ntu.edu.sg

ABSTRACT

Multichannel high electron mobility transistor (MC-HEMT) heterostructures are one of the choices for improved power performance of GaN HEMTs. By comparing the experimentally obtained two-dimensional electron gas (2DEG) concentration of unintentionally doped (UID) AlGaN/GaN MC-HEMTs with simulated 2DEG concentration, we hypothesized that hole trap(s) exist at the buried GaN/AlGaN interfaces, which act as sources of 2DEG in UID MC-HEMT heterostructures. Furthermore, these hole traps stop the Fermi level from cutting the valence band at GaN/AlGaN interfaces, which in turn precludes the generation of parallel two-dimensional hole gas (2DHG) in the MC-HEMT. However, no experimental report is present as a proof for the existence of such a hole trap in MC-HEMT heterostructures. In this study, a capacitance–conductance method on single and dual channel HEMTs revealed traps with higher time constant of 19–28.7 μs exclusively for the dual channel HEMT heterostructure. These traps are observed at the buried GaN/AlGaN interface of the dual channel HEMT; hence, they are attributed to possible hole traps at this interface. By conducting systematic deep level transient spectroscopy measurements, the existence of hole traps is confirmed at the buried GaN/AlGaN interface with an activation energy of 717 meV and a capture cross section of 1.3×10^{-14} cm^2. This experimental evidence of the existence of hole traps at the GaN channel/AlGaN interface further supports our claim that these hole traps act as the source of 2DEG in UID MC-HEMTs and that buried parallel 2DHG channels do not exist in MC-HEMTs.

The AlGaN/GaN based multichannel high electron mobility transistor (MC-HEMT)[1] is one of the approaches that has the potential to achieve higher power operations compared to a single channel conventional AlGaN/GaN HEMT.[2,3] Parallel conducting multi two-dimensional electron gas (2DEG) channels in AlGaN/GaN MC-HEMTs reduce the net effective sheet resistance leading to lower on-resistance and improved power performance, while maintaining the higher breakdown voltages and other important characteristics of AlGaN/GaN HEMTs. Various groups have demonstrated a modulation doped and unintentionally doped (UID) AlGaN/GaN based MC-HEMT heterostructure using MOCVD growth technique.[1,2,4–6] Recently, our group also demonstrated UID AlGaN/GaN MC-HEMT heterostructures using plasma-assisted molecular beam epitaxy (PAMBE).[7]

In our work,[7] by comparing the experimentally obtained cumulative 2DEG concentration with the Poisson–Schrödinger (PS) simulated 2DEG concentration, we hypothesized that donor type hole trap states exist at 0.6–0.8 eV above the valence band of buried GaN

channel/AlGaN interfaces, which not only act as sources of 2DEGs in MC-HEMTs but also eliminate the possibility of hole gas formation at the GaN/AlGaN interface. However, to validate this hypothesis, experimental evidence of the hole trap at the buried GaN/AlGaN interface of AlGaN/GaN MC-HEMT is necessary. Hole traps were detected at the AlGaN/GaN interface of N-polar HEMT heterostructures[8] and at the interface of Ga-polar InGaN/GaN heterostructures.[9–11] Till date, trap studies on Ga-polar III-nitride MC-HEMT heterostructures neither reveal any such hole trap nor identify its location in this heterostructure.[12,13] In this study, through capacitance–conductance and deep level transient spectroscopy (DLTS) studies, we demonstrate the existence of hole traps at the buried GaN/AlGaN interface in the AlGaN/GaN dual channel HEMT heterostructure. A dual channel instead of multichannel reduces the complexity but still provides the necessary epi-structure to probe the hole trap at the buried-GaN/AlGaN interface. Such a proof further confirms our hypothesis of buried hole trap states at the GaN/AlGaN interface acting as sources of 2DEGs in MC-HEMTs and that buried parallel 2DHG channels do not exist in MC-HEMTs.

For this study, two samples were grown using PAMBE growth technique. Sample 1 is an UID AlGaN/GaN single channel HEMT heterostructure, and sample 2 is an AlGaN/GaN dual channel HEMT heterostructure, as shown in Figs. 1(a) and 1(b), respectively. For both samples, the epistructure growth started with a 100 nm thick AlN nucleation layer, grown in extremely N-rich growth conditions (III/V $\ll 1$) to avoid Si carry over from the SiC substrate to the GaN buffer.[14] The GaN buffer layer growth was performed in slightly metal rich growth condition (III/V > 1) with sequential growth interruptions to evaporate the accumulated Ga on the surface.[15,16] Subsequently, for both samples, GaN cap and AlGaN barrier layers were grown in metal rich growth conditions. Figures 1(c) and 1(d) show the experimentally obtained capacitance–voltage (C–V) and conductance–voltage (G–V) characteristics at 1 MHz, on samples 1 and 2, respectively. C–V and G–V measurements were performed on a circular Ni (40)/Au (250 nm) Schottky diode of 300 μm diameter with surrounded Ohmic contact of Ti (20 nm)/Al (120 nm)/Ni (40 nm)/Au (250 nm).

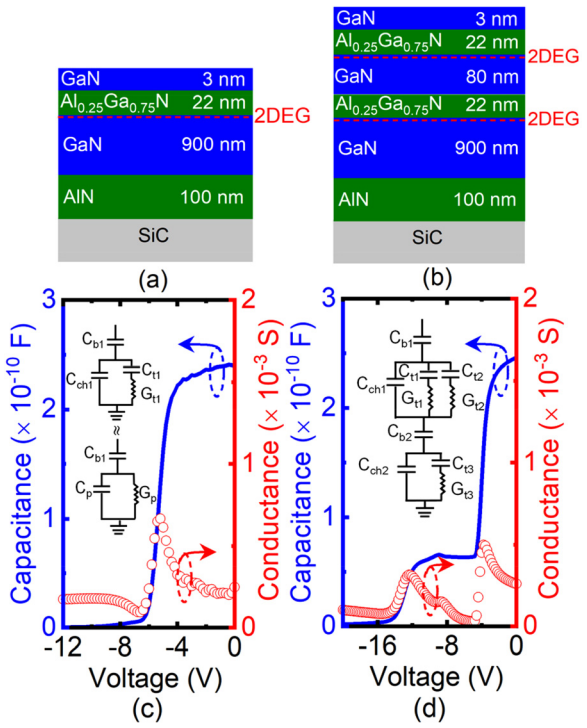

FIG. 1. Schematic cross section of heterostructure of samples 1 (a) and 2 (b). Capacitance–voltage (C–V) and conductance–voltage (G–V) measurements at 1 MHz of samples 1 (c) and 2 (d).

The trap state properties are analyzed using the capacitance–conductance method, similar to the well-established technique of Nicollian and Goetzberger,[17] where parallel trap conductance as a function of frequency is studied at various applied bias. The equivalent circuit of a single channel HEMT heterostructure is shown in the inset of Fig. 1(c). The barrier capacitance C_{b1} of the HEMT is equivalent to the insulator capacitance in the Si–SiO_2 structure of Ref. 17. Similarly, the series of trap capacitance (C_{t1}) and trap conductance (G_{t1}) can be shown to be in parallel with channel capacitance (C_{ch1}). Here, C_{t1} and G_{t1} represent the equivalent trap capacitance and conductance of several traps present at the first AlGaN/GaN interface. This parallel circuit further can be simplified as an equivalent parallel circuit of C_p and G_p, as presented in inset of Fig. 1(c). Hence, as suggested in Ref. 17, C_p and G_p can be expressed as

$$C_p = C_{b1} + \frac{qD_{it1}}{\omega\tau_{it1}\tan(\omega\tau_{it1})}, \tag{1}$$

$$\frac{G_p}{\omega} = \frac{qD_{it1}}{2\omega\tau_{it1}} ln\left[1 + (\omega\tau_{it1})^2\right], \tag{2}$$

where $\omega = 2\pi f$ is the radial frequency, C_{b1} is the barrier capacitance, τ_{it1} is the interface trap time constant, and D_{it1} is the density of trap states. However, in general, C–V and G–V measurements from the fabricated diodes were obtained by assuming parallel capacitance (C_m)–conductance (G_m) setup in the capacitance measurement tool. Here, C_m and G_m are the measured capacitance and parallel conductance, respectively. Measurements were performed with frequencies varying from 1 kHz to 2 MHz. The measured conductance (G_m) needs to be converted back to $\frac{G_p}{\omega}$ to use Eq. (2) for the extraction of trap time constant. Conversion of G_m to $\frac{G_p}{\omega}$ resulted as

$$\frac{G_p}{\omega} = \frac{\omega G_m C_{b1}}{G_m^2 + \omega^2(C_{b1} - C_m)^2}. \tag{3}$$

In HEMT heterostructures, by varying the applied bias, trap properties at various interfaces can be extracted.[18–20] This spatial analysis of trap information is important to understand the exact position of the traps in the heterostructure. Figures 2(a) and 2(b) show the carrier concentration estimated from C–V measurements and the applied bias as a function of the heterostructure thickness of samples 1 and 2, respectively. To probe the trap properties at the AlGaN/GaN interface and the GaN channel layer in sample 1, it is necessary to deplete the 2DEG and keep the applied bias within -5.5 to < -7 V as shown in Figs. 1(c) and 2(a). Within this applied bias, depth profile remained in GaN buffer, and the modulation of Fermi level reveals the corresponding trap states, whose capacitance and conductance series comes in parallel with GaN channel capacitance. The scattered points in Fig. 2(c) showed the $\frac{G_p}{\omega}$ as a function of ω obtained using Eq. (3) for sample

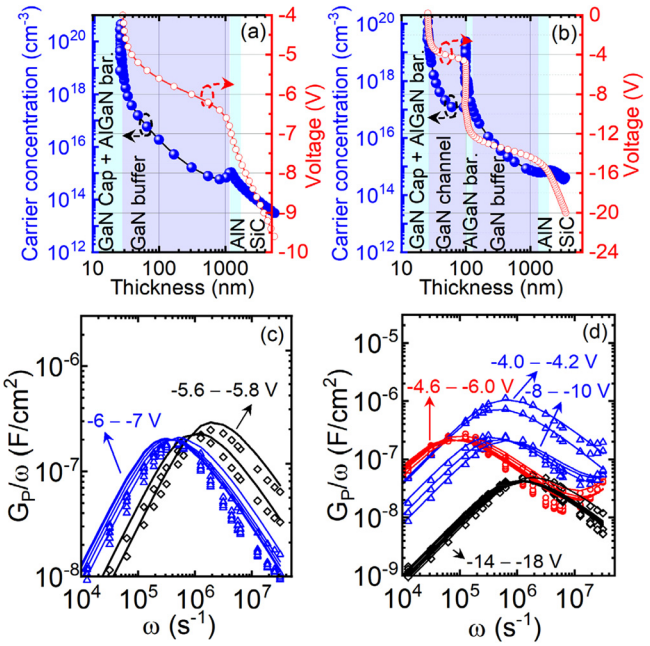

FIG. 2. Carrier concentration and the applied bias as a function of the heterostructure thickness of samples 1 (a) and 2 (b). The obtained and fitted $\frac{G_p}{\omega}$ as a function of ω for samples 1 (c) and 2 (d).

1. The scattered points are fitted using Eq. (2), shown as line plots, and the obtained trap time constant (τ) and trap density (Dτ) are listed in Table I. Based on the time constants obtained, the traps were broadly categorized into two types, namely, trap 1 and trap 2 with time constants of 0.97–1.87 and 3.8–6.3 μs, respectively. As shown in Fig. 2(c), trap 1 was observed at lower applied bias of −5.6 to −5.8 V, whereas trap 2 was observed at higher applied bias of −6 to −7 V.

The equivalent circuit of a dual channel HEMT heterostructure is shown in the inset of Fig. 1(d). In this case, the trap capacitance (C_{t1}) and conductance (G_{t1}) at the AlGaN/GaN channel interface connects in parallel with the equivalent trap capacitance (C_{t2}) and trap conductance (G_{t2}) of several traps at the GaN channel/AlGaN (2nd barrier) interface. This combination connects in parallel with GaN channel capacitance (C_{ch1}). Similar to sample 1, to probe the trap properties of sample 2 at the AlGaN/GaN channel interface, in the GaN channel, and at the GaN channel/AlGaN barrier interface, it is necessary to deplete the top 2DEG and keep the applied bias within −4 to $<$ −10 V as shown in Figs. 1(d) and 1(b). As shown in Fig. 2(d), the plots of $\frac{G_p}{\omega}$ as a function of ω revealed two types of traps within the applied bias range, and the corresponding extracted trap time constant and trap density are listed in Table I. With the applied bias of $<$−4.2 V, traps similar to trap 2 in sample 1 were revealed. With the increased applied bias of −4.6 to −6.0 V, a newer trap, trap 3, with higher time constant of 19–28.7 μs was revealed. However, with further increase in the applied bias of −8 to −10 V, trap similar to the trap 2 in sample 1 was revealed. When the applied bias is beyond −14 V, the second 2DEG depletes, which allows the probing of GaN buffer. As shown in Fig. 2(d), trap similar to the trap 1 in sample 1 was revealed when the applied bias was −14 to −18 V. Here, the traps 2 and 1 are similar to the traps observed at AlGaN/GaN interface or in the GaN buffer of sample 1. However, considering the applied bias of −4.6 to −6.0 V as shown in Fig. 2(b), the newer trap, the trap 3, must have been originated from the GaN channel/AlGaN interface, as such a high time constant was also not observed in sample 1. If so, the newer trap could possibly be the hypothesized hole trap originated at GaN/AlGaN interface. When the applied bias is lower or higher than the range of −4.6 to −6.0 V, trap 3 signature disappears and trap 2 always prevails, possibly from the first GaN channel or AlGaN/GaN channel interface. This also suggests that the proposed hole trap state may not possibly be extended over a longer range within the bandgap at the GaN channel/AlGaN interface.

The capacitance–conductance studies possibly gave an indication of the presence of hole trap at GaN channel/AlGaN interface and indicated the applied bias required to probe them. Though hole trap states prevail in certain bias range, the measured conductance is always a parallel combination of conductance due to electron traps observed at the AlGaN/GaN channel and hole traps at GaN channel/AlGaN interfaces as shown in the equivalent circuit in Fig. 1(d). Hence, to decouple the hole and electron traps at these interfaces and extract their activation energies, DLTS measurements were performed on the Schottky barrier diode of sample 2. DLTS measurements were conducted using Semilab DLS-83D measurement tool with lock-in function and signal-integration. To reveal and understand the hole trap state and position, three experiments were performed with three applied reverse bias conditions and probing pulses. To obtain the activation energy and capture cross section for different trap states, the lock-in amplifier frequency was varied for each experimental bias condition in DLTS measurement. Self-consistent Poisson–Schrödinger simulation software, Bandeng,[21] was used to determine the band structure and charge distribution in sample 2 for analyzing the band structure configuration of each DLTS experimental condition.

The first set of DLTS experiments were performed using an applied reverse bias of −4.5 V and a probing pulse of −0.5 V. Figure 3(a) shows the energy band diagram of the GaN cap/AlGaN/GaN/AlGaN interfaces of sample 2 at the applied reverse and probing biases. Figure 3(b) shows corresponding DLTS signal obtained at a lock-in frequency of 1720 Hz. As shown in the figure, two electron traps, namely E2 and E4, were identified. The corresponding trap state activation energy and capture cross section are listed in Table II. As shown in Fig. 3(a), with the applied reverse bias of −4.5 V, the top 2DEG gets partially depleted and gets filled back with the probing pulse. Moreover, as show in Fig. 3(a), these biases do not also

TABLE I. Time constant (τ) and trap density (Dτ) of traps 1, 2, and 3 of samples 1 and 2.

Sample	τ_1 (10^{-6} s)	Dτ_1 ($\times 10^{12}$ cm^{-2}/eV)	τ_2 (10^{-6} s)	Dτ_2 ($\times 10^{12}$ cm^{-2}/eV)	τ_3 (10^{-6} s)	Dτ_3 ($\times 10^{12}$ cm^{-2}/eV)
1	0.97–1.87	3.6–2.9	3.8–6.3	2.55–6.22	...	...
2	1.1–1.93	0.64–0.76	3.0–5.6	3.22–3.44	19–28.7	3.38–3.94

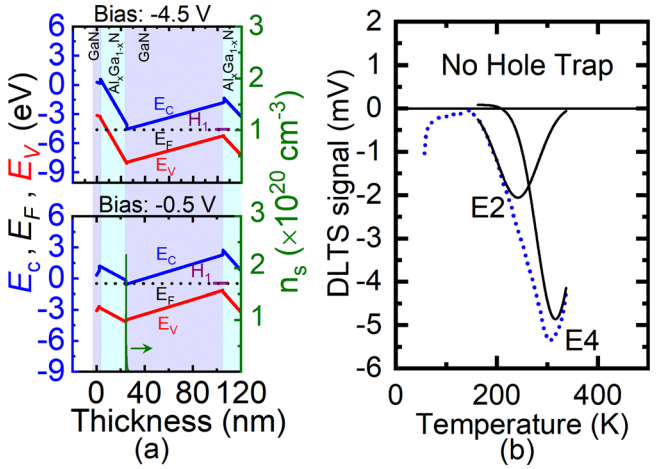

FIG. 3. Energy band diagrams of the GaN cap/AlGaN/GaN/AlGaN interfaces of sample 2 at an applied reverse and probing biases of −4.5 and −0.5 V, respectively, (a). DLTS signal obtained at lock-in frequency of 1720 Hz for sample 2 (b).

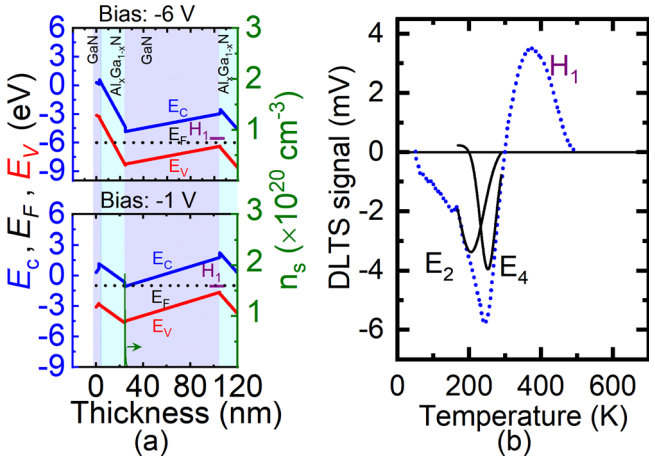

FIG. 4. Energy band diagrams of the GaN cap/AlGaN/GaN/AlGaN interfaces of sample 2 at an applied reverse and probing biases of −6 and −1 V, respectively, (a). DLTS signal obtained at lock-in frequency of 1432 Hz for sample 2 (b).

modulate hole trap, H1, at the GaN/AlGaN interface. Hence, traps observed with these experimental conditions could have been originated anywhere from the GaN cap, AlGaN barrier, or AlGaN/GaN interface. No hole trap observation with this applied reverse bias is consistent with the conductance measurements.

In the conductance measurements, trap 3 (possibly the hole trap) was observed for an applied bias range of −4.6 to −6 V. Hence, the second set of DLTS experiments was conducted using an applied reverse bias of −6 V and a probing pulse of −1.0 V. As shown in Fig. 2(b), an applied bias of −6 V allows probing of traps at negatively polarized GaN/AlGaN interface. Figures 4(a) and 4(b) show the corresponding energy band diagrams and DLTS signal, respectively. Comparison of the energy band diagram of Fig. 4(a) with Fig. 3(a) also suggests that in addition to the electron traps revealed from GaN cap or AlGaN barrier or AlGaN/GaN interface (revealed in the first set of DLTS), hole traps at GaN/AlGaN interface must be revealed from GaN/AlGaN interface under this probing condition. As shown in Fig. 4(b), along with the electron traps, which could possibly be E2 and E4, a hole trap, H1, with a strong positive signal is observed. As listed in Table II, the hole trap showed an activation energy of 717 meV with a capture cross section of 1.3×10^{-14} cm^2. It should be noted that the observation of hole trap in DLTS measurements matches with the observation of higher time constant trap, trap 3, at the applied biases of −4.6 to −6 V in conductance experiments.

TABLE II. Activation energy and capture cross section of various traps, obtained using DLTS.

Applied reverse bias (V)/ probing pulse (V)	E_{act} (meV)	σ (cm^2)	Traps
−4.5/−0.5	−243	2.5×10^{-18}	E2
	−461	3.4×10^{-16}	E4
−6.0/−1.0	717	1.3×10^{-14}	H1
−8.0/−5.0	−92	6.4×10^{-21}	E1
	−395	7.1×10^{-18}	E3
	−525	2.6×10^{-17}	E5

The third set of DLTS experiments was performed using an applied reverse bias of −8 V and a probing pulse of −5.0 V. As shown in Fig. 2(b), an applied bias of −8 V still allows probing of traps at the GaN/AlGaN interface. Figures 5(a) and 5(b) show the corresponding energy band diagram at each bias and DLTS signal, respectively. As shown in Fig. 5(a), if the hole traps spread over a longer range above the valence band at the GaN/AlGaN interface, the combination of applied and probing biases of −8 and −5 V could modulate those hole traps and reveal them. As shown in Fig. 5(b), the electron traps, namely, E1, E3, and E5, were only observed. Table II lists the trap activation energy of these traps along with their capture cross sections. Some of the electron traps observed can be correlated with traps reported for GaN bulk or epitaxial layers in SH- and DH-HEMT

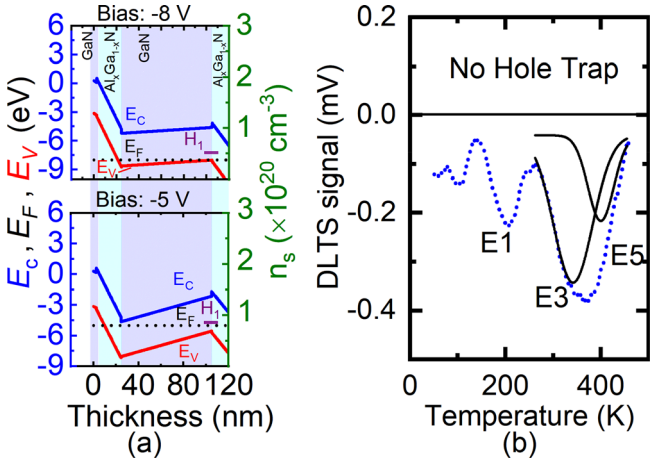

FIG. 5. Energy band diagrams of the GaN cap/AlGaN/GaN/AlGaN interfaces of sample 2 at an applied reverse and probing biases of −8 and −5 V, respectively, (a). DLTS signal measured at the lock-in frequency of 1472 Hz for sample 2 (b).

heterostructures.[18,22–24] However, the focus of this work is to study hole trap at the GaN/AlGaN interface. The absence of positive signal in DLTS confirms that hole traps are not extending over longer range within the bandgap at the GaN channel/AlGaN interface, which is again consistent with the conductance experiments. From the energy band diagram in Fig. 5(a), it can be deduced that all the electron trap states should originate from the AlGaN/GaN interface and the GaN channel layer. In the literature, reports suggested that hole traps could also be originated from the AlGaN barrier.[22,25,26] However, as shown in Figs. 3(a) and 5(a), the DLTS experiments 1 and 3 completely probed the top AlGaN barrier and no hole traps were detected from the AlGaN barrier layer or top AlGaN/GaN interface.

In summary, using capacitance–conductance and DLTS measurements, a hole trap state at 717 meV above valence band is observed at the buried GaN/AlGaN interface in the dual channel HEMT heterostructure. This experimental evidence of hole trap at the GaN/AlGaN interface confirms our hypothesis[7] of the existence of such trap state, which acts as the origin of 2DEG in MC-HEMT heterostructures, and the buried parallel 2DHG channel at negatively polarized GaN/AlGaN interface does not exist in these structures.

We acknowledge and thank the Semilab ZRT Budapest team for their great support for getting DLTS data of this study. The authors gratefully acknowledge the funding support from the Ministry of Education, Singapore (Award No. RG128/22).

AUTHOR DECLARATIONS

Conflict of Interest

The authors have no conflicts to disclose.

Author Contributions

Ravikiran Lingaparthi: Conceptualization (equal); Data curation (equal); Formal analysis (equal); Investigation (equal); Methodology (equal); Writing – original draft (equal); Writing – review & editing (equal). **Nethaji Dharmarasu:** Conceptualization (equal); Formal analysis (equal); Resources (equal); Supervision (equal); Writing – review & editing (equal). **K. Radhakrishnan:** Formal analysis (equal); Funding acquisition (equal); Resources (equal); Supervision (equal); Validation (equal); Writing – review & editing (equal). **Lili Huo:** Data curation (supporting); Formal analysis (supporting); Investigation (supporting).

DATA AVAILABILITY

The data that support the findings of this study are available from the corresponding author upon reasonable request.

REFERENCES

[1]S. Heikman, S. Keller, D. S. Green, S. P. DenBaars, and U. K. Mishra, J. Appl. Phys. **94**(8), 5321 (2003).
[2]J. Chang, S. Afroz, K. Nagamatsu, K. Frey, S. Saluru, J. Merkel, S. Taylor, E. Stewart, S. Gupta, and R. Howell, IEEE Electron Device Lett. **40**(7), 1048 (2019).
[3]L. Nela, M. Xiao, Y. Zhang, and E. Matioli, Appl. Phys. Lett. **120**(19), 190501 (2022).
[4]C. Middleton, S. Dalcanale, J. W. Pomeroy, M. J. Uren, J. Chang, J. Parke, I. Wathuthanthri, K. Nagamatsu, S. Saluru, S. Gupta, R. Howell, and M. Kuball, IEEE Electron Device Lett. **40**(9), 1374 (2019).
[5]J. Ma, C. Erine, P. Xiang, K. Cheng, and E. Matioli, Appl. Phys. Lett. **113**(24), 242102 (2018).
[6]C. Erine, J. Ma, G. Santoruvo, and E. Matioli, IEEE Electron Device Lett. **41**(3), 321 (2020).
[7]R. Lingaparthi, N. Dharmarasu, K. Radhakrishnan, A. Ranjan, T. L. A. Seah, and L. Huo, Appl. Phys. Lett. **118**(12), 122105 (2021).
[8]S. Rajan, A. Chini, M. H. Wong, J. S. Speck, and U. K. Mishra, J. Appl. Phys. **102**(4), 044501 (2007).
[9]C. A. Schaake, D. F. Brown, B. L. Swenson, S. Keller, J. S. Speck, and U. K. Mishra, Semicond. Sci. Technol. **28**(10), 105021 (2013).
[10]J. W. Kim, G. H. Song, and J. W. Lee, Appl. Phys. Lett. **88**(18), 182103 (2006).
[11]Z. Q. Fang, D. C. Look, C. Lu, and H. Morkoç, J. Electron. Mater. **29**(9), L19 (2000).
[12]K. Zhang, J. Xue, M. Cao, L. Yang, Y. Chen, J. Zhang, X. Ma, and Y. Hao, J. Appl. Phys. **113**(17), 174503 (2013).
[13]S. K. Jha, C. Surya, K. J. Chen, K. M. Lau, and E. Jelencovic, Solid-State Electron. **52**(5), 606 (2008).
[14]W. E. Hoke, A. Torabi, J. J. Mosca, R. B. Hallock, and T. D. Kennedy, J. Appl. Phys. **98**(8), 084510 (2005).
[15]K. Radhakrishnan, N. Dharmarasu, Z. Sun, S. Arulkumaran, and G. I. Ng, Appl. Phys. Lett. **97**(23), 232107 (2010).
[16]R. Aidam, P. Waltereit, L. Kirste, M. Dammann, and R. Quay, Phys. Status Solidi A **207**(6), 1450 (2010).
[17]E. H. Nicollian and A. Goetzberger, Bell Syst. Tech. J. **46**(6), 1055 (1967).
[18]X.-H. Ma, J.-J. Zhu, X.-Y. Liao, T. Yue, W.-W. Chen, and Y. Hao, Appl. Phys. Lett. **103**(3), 033510 (2013).
[19]X.-H. Ma, W.-W. Chen, B. Hou, K. Zhang, J.-J. Zhu, J.-C. Zhang, X.-F. Zheng, and Y. Hao, Appl. Phys. Lett. **104**(9), 093504 (2014).
[20]J.-J. Zhu, X.-H. Ma, B. Hou, W.-W. Chen, and Y. Hao, AIP Adv. **4**(3), 037108 (2014).
[21]See http://my.ece.ucsb.edu/mgrundmann/bandeng.htm for M. J. Grundmann, "BandEng Software, University of California Santa Barbara" (2020).
[22]A. Y. Polyakov and I.-H. Lee, Mater. Sci. Eng. **94**, 1 (2015).
[23]Z.-Q. Fang, D. C. Look, P. Visconti, D.-F. Wang, C.-Z. Lu, F. Yun, H. Morkoç, S. S. Park, and K. Y. Lee, Appl. Phys. Lett. **78**(15), 2178 (2001).
[24]Y. He, P. Li, C. Wang, X. Li, S. Zhao, M. Mi, J. Pei, J. Zhang, X. Ma, and Y. Hao, Appl. Phys. Lett. **107**(6), 063501 (2015).
[25]A. R. Arehart, A. A. Allerman, and S. A. Ringel, J. Appl. Phys. **109**(11), 114506 (2011).
[26]Z.-Q. Fang, B. Claflin, D. C. Look, D. S. Green, and R. Vetury, J. Appl. Phys. **108**(6), 063706 (2010).